JOURNAL OF SOLID STATE CHEMISTRY 17, 343–352 (1976)

# Phase Equilibria in the System $MnO–TiO_2–Ti_2O_3$ at 1473°K

I. E. GREY, C. LI, AND A. F. REID

*CSIRO Division of Mineral Chemistry, P.O. Box 124, Port Melbourne, Victoria 3207, Australia*

Received September 23, 1975

The oxygen fugacity-composition isotherm at 1473°K has been established for the $MnO–TiO_2–Ti_2O_3$ system for $f_{O_2}$ in the range $10^{-13.5}$–$10^{-18}$ atm. The quenching method was used and control of oxygen fugacity was achieved with $CO_2/H_2$ mixtures. Phase equilibria results are presented for the reduced rutile Magneli phases, $Ti_nO_{2n-1}$–$MnTi_{n-1}O_{2n-1}$, and for the partial solid solutions $Ti_3O_5$–"$MnTi_2O_5$" ($M_3O_5$), $Ti_2O_3$–$MnTiO_3$ (α-oxide), and $MnTi_2O_4$–$Mn_2TiO_4$ (spinel). Loss of manganese by volatilization is a problem in this system at low oxygen fugacities.

## 1. Introduction

We have recently reported the application of phase equilibria data to an interpretation of ilmenite reduction (*1*). It was shown that the phase diagram for the Fe–Ti–O system was inadequate for describing the reaction sequences in the reduction of *natural* ilmenites, containing 1 or 2% manganese. Even such a small amount of the fourth component can have a marked effect because the MnO remains unreduced while iron is separated from the oxides as metal. Thus, as reduction proceeds, manganese concentrates in an oxide phase assemblage bounded by the compositions $FeO–MnO–TiO_2–Ti_2O_3$. Analyses of reduction products taken from a commercial ilmenite upgrading plant show approximately equal concentrations of iron oxide and manganese oxide in the phase assemblage remaining after metallic iron has been leached out (*2*).

An understanding of the reaction sequences occurring in the reduction of natural (West Australian) ilmenites thus requires a knowledge of the phase diagram for the quaternary system Mn–Fe–Ti–O. As part of a study of this complex system we have investigated phase equilibria in the $MnO–TiO_2–Ti_2O_3$ system at 1473°K, using the quench method. We report here the results of a controlled atmosphere study for oxygen fugacities in the range $10^{-13.5}$–$10^{-18}$ atm.

## 2. Previous Work

Very little work has been published on the phase equilibria of the $MnO–TiO_2–Ti_2O_3$ system, although the three associated binary systems have been studied in some detail. The system $TiO_2–Ti_2O_3$ has been investigated over a wide temperature range, 1173–1873°K, using sealed tube experiments (*3*, *4*), controlled atmosphere quench methods (*5*, *6*, *11*), thermogravimetry (*7–9*), and solid state emf studies (*10*). At the temperature of our study the end member phases have, respectively, rutile and corundum-type structures with composition ranges of $TiO_{2.00}$ to $TiO_{1.99}$ and $TiO_{1.49}$ to $TiO_{1.51}$ (*3*). Adjacent to $Ti_2O_3$ is $Ti_3O_5$, with a distorted pseudobrookite structure and a very narrow range of homogeneity (*3*). The composition range $TiO_{1.67}$ to $TiO_{1.99}$ is spanned by series of crystallographic shear structures derived from the rutile structure type (*11*). Between $TiO_{1.67}$ and $TiO_{1.889}$ the seven discrete phases with general formula $Ti_nO_{2n-1}$, $n = 3$–9, are known as Magneli phases. The thermodynamics of these phases

have been well characterized by a number of workers (*5–10*).

In the $MnO–TiO_2$ system, the end member compound MnO has a region of nonstoichiometry extending to $MnO_{1.06}$ at 1473°K (*12*). The binary system has two stable compounds: $MnTiO_3$ with ilmenite structure and $Mn_2TiO_4$ with spinel structure (*13*). The only reported compound in the $MnO–Ti_2O_3$ system is the spinel, $MnTi_2O_4$ (*14*).

In the ternary $MnO–TiO_2–Ti_2O_3$ system, $MnTi_2O_4$ and $Mn_2TiO_4$ form a continuous spinel solid solution series at 1473°K (*14*). We have previously reported results for the α-oxide solid solution ($MnTiO_3–Ti_2O_3$) and $M_3O_5$(ss) solid solution ($Ti_3O_5$–"$MnTi_2O_5$"), from sealed tube equilibration studies (*1*). The α-oxide solid solution has a large miscibility gap at 1473°K extending from about 10 to 75 mole% $Ti_2O_3$. The $M_3O_5$(ss) extends from 0 to 65 mole% of the hypothetical compound, $MnTi_2O_5$ in $Ti_3O_5$. There have been no data published on ternary solid solutions of any of the reduced rutile or Magneli phases.

## 3. Experimental

### *3.1. Gas Equilibration Studies*

Phase equilibria at 1473°K in the $MnO–TiO_2–Ti_2O_3$ system were determined by the quenching technique. Suitable mixtures of $Mn_2O_3$ and $TiO_2$ were equilibrated at a controlled oxygen fugacity for 1–3 days and then rapidly quenched in an inert atmosphere. The phases present were determined by X-ray diffraction and compositions of phase assemblages estimated from chemical analyses. Fisher certified reagent titanium dioxide (anatase) was dried at 1073°K for 2 days prior to use, and $Mn_2O_3$ was prepared by decomposition of A.R. $MnCl_2.6H_2O$ in air at 923°K.

Control of oxygen fugacities was achieved by mixing carbon dioxide and hydrogen in various ratios by use of calibrated flow meters (*15*). The analytical grade carbon dioxide had a purity of 99.99% ($H_2O$ < 30 ppm; air < 100 ppm). The hydrogen used was of high purity. As our studies were mainly at low oxygen fugacities, corresponding to high hydrogen/carbon dioxide ratios, we further purified the hydrogen by passage through B.T.S. catalyzer (active copper on alumina substrate) then through molecular sieves.

The equilibration runs were carried out in a horizontal closed-end Alsint alumina tube fitted with a water-cooled quench-end made of brass. This design, similar to that described by Webster and Bright (*16*), allows efficient preheating of the gas mixture through the inlet tube which extends to the closed end of the work tube (*6*). Heat was supplied by a horizontal platinum wound furnace; temperature stability to ±0.5°K was maintained with a Transitrol (Ether Ltd., United Kingdom) potentiometric controller. Temperatures were measured with a calibrated Pt/Pt–13% Rh thermocouple.

The sample pellets were contained in a molybdenum boat fitted with a molybdenum draw wire by which the samples could be rapidly withdrawn from the hot zone. Quenching was facilitated with liquid nitrogen, which was directed onto the sample through ports in the brass quench end.

Further details concerning the experimental apparatus and procedure, as well as an analysis of the accuracy of results obtained using this method are given in (*6*). The maximum uncertainty in $\log f_{O_2}$ is estimated to be ±0.05 (*6*).

### *3.2. Chemical Analyses*

The samples were analyzed for total manganese and titanium and trivalent titanium. For total manganese and titanium, the samples were fused with sodium bisulphate to render them acid soluble. Total manganese was determined by potentiometric titration with potassium permanganate in neutral pyrophosphate solution. The total titanium content was obtained by reduction to the trivalent state with aluminium followed by titration with standardized ferric alum.

For the trivalent titanium determination the sample was dissolved in a hydrofluoric–sulfuric acid solution containing excess pentavalent vanadium. The Ti(III) content was determined by back titration of the excess vanadium(V) with standard ferrous sulphate solution. Ti(III) was also determined from the increase in weight of the sample after heating to constant weight at 1323°K. We

verified that there was no oxidation of Mn(II) in the presence of titanium at this temperature by heating a sample of $MnTiO_3$ along with the reduced samples. There was no detectable change in weight of $MnTiO_3$ after heating periods of up to 48 hr. $Mn^{2+}$, $Ti^{3+}$, and total Ti contents were estimated to be determined to within $\pm 0.5\%$.

### 3.3. *X-Ray Diffraction*

X-ray powder diffraction patterns were obtained with a Philips diffractometer fitted with a graphite monochromator and using Cu$K\alpha$ radiation. Silicon was used as an internal standard for lattice parameter determination, and slow scan rates (0.25°/min) ensured high precision in the data.

## 4. Limitations of the Gas Equilibration Study: Volatilization of Manganese at Low Oxygen Activities

A possible source of major errors in thermodynamic studies of multicomponent systems at elevated temperatures is the partial loss of a component by volatilization. Such a possibility could be overlooked easily if the volatile phase did not have a counterpart in the condensed system being studied, e.g., loss of a component as gaseous *metal* from a condensed system consisting only of *metal oxides*. Such a situation occurs in the manganese–oxygen system; at temperatures near 1473°K the fugacity of gaseous manganese above solid MnO can be up to $10^7$ times greater than the fugacity of gaseous MnO. The extent of volatilization of metallic manganese vapor from the solid oxide is a function of both temperature and oxygen fugacity. The relationships between the equilibrium fugacities of the volatile species over the condensed oxide and elemental phases and the oxygen fugacity at a fixed temperature are best illustrated using $\log f_{MnO_x}$ vs $\log f_{O_2}$ diagrams. These diagrams were first used extensively by Kellogg (*17*) and Jansson and Gulbransen (*18*). Using published thermodynamic data (*19–21*), we calculated the various $\log f_{MnO_x}$ vs $\log f_{O_2}$ relationships for the Mn–O system at 1473°K, using a computer program written by Dr. A. G. Turnbull. These are given in Fig. 1. The

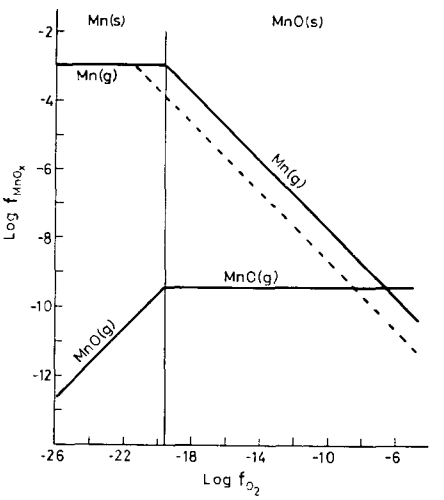


FIG. 1. Thermochemical diagram for the Mn–O system at 1473. Fugacities of gaseous Mn and MnO above solid Mn and MnO as a function of the oxygen fugacity. The dashed line represents the fugacity of gaseous Mn above the hypothetical compound $MnTi_2O_5$.

fugacity of gaseous MnO above solid MnO is $10^{-9.45}$ atm. It is independent of oxygen fugacity, and loss of MnO as gaseous oxide would be negligible over reaction periods of a few days. However, the fugacity of elemental manganese over solid MnO increases with decreasing oxygen fugacity; at low oxygen fugacities considerable loss by volatility will occur. The seriousness of the problem may be illustrated with an example. Consider a 0.5 g pellet of MnO equilibrated in a flowing gaseous atmosphere (flow rate = 0.5 liter $min^{-1}$) for 2 days. If it is assumed that the gas flow is saturated with elemental vapor, the Ideal Gas law may be used together with the data in Fig. 1 to calculate the loss of manganese from the pellet as a function of oxygen fugacity. The calculations show that if one wishes to keep the loss of manganese at less than 0.5% of the original manganese content (i.e., corresponding approximately to the error in determination of manganese by chemical analysis) then the oxygen fugacity must be kept higher than $10^{-14}$ atm. In the ternary Mn–Ti–O system, the presence of titanium oxide results in a lowering of the activity of solid MnO with a concomitant reduction in the

fugacities of the vapour phases as shown by the dotted line in Fig. 1. From a study of analyses on a large number of samples it was concluded that losses of manganese by volatilization at 1473°K were negligible from samples with a Mn/(Mn + Ti) ratio less than 0.5 when equilibrated at oxygen fugacities higher than about $10^{-17}$ atm for periods up to 2 days. Although samples were sometimes studied outside these limits (see Fig. 2) and characterized with complete analyses, the results are probably not very precise because the continuing process of volatilization may preclude complete equilibration.

The use of $CO_2/H_2$ mixtures in general restricted the oxygen fugacity range of the study, to values above $10^{-17.5}$ atm, since carbon deposition occurs below this value. Some equilibrations were carried out in hydrogen only.

Because of the manganese volatilization problem, this study is mainly concerned with the investigation of the reduced rutile phases and the $Ti_3O_5$–"$MnTi_2O_5$" solid solution series, which have equilibrium oxygen fugacities higher than $\sim 10^{-17}$ atm. A parallel study of those regions of the $MnO$–$Ti_2O_3$–$TiO_2$ system which equilibrate at lower oxygen fugacities is being made by the sealed silica tube technique and will be reported elsewhere. However, certain of the sealed tube results pertinent to the present work have been included here.

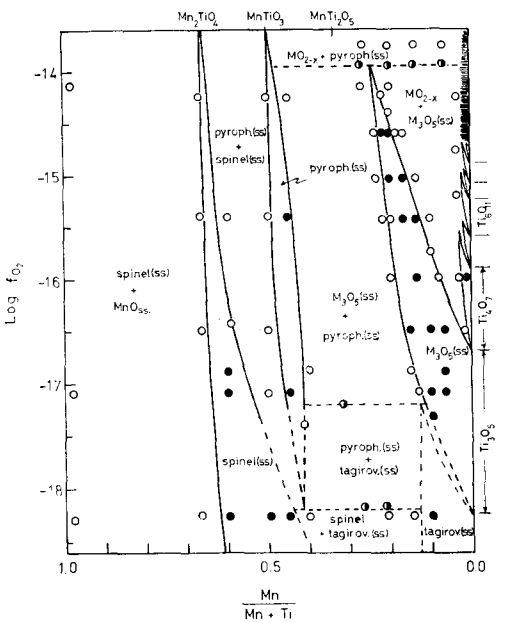


FIG. 2. Oxygen fugacity vs composition for the Mn–Ti–O system at 1473°K and for Mn/(Mn + Ti) ratios between 0.00 and 1.00. Circles represent experimental data. ●, single phase regions; ○, two-phase regions; ◑, three phase regions. Pyroph. and tagirov. refer to pyrophanite(ss) and tagirovite(ss). (See Section 5.3.)

## 5. Results and Discussion

The results of the equilibration experiments are shown in Fig. 2 as a plot of oxygen fugacitv vs the metal atom ratio, expressed as Mn/(Mn + Ti). This diagram gives no explicit information on the oxygen content of the

TABLE I

THERMODYNAMIC DATA FOR $MnO$–$TiO_2$–$Ti_2O_3$ AT 1200°C; INVARIANT OXYGEN FUGACITIES FOR THREE (SOLID) PHASE EQUILIBRIA

| $f_{O_2}$ (atm) | Equilibrium phases | Composition of phases |
|---|---|---|
| $10^{-13.95}$ | α-oxide | $MnTiO_3$ |
| | + $M_3O_5$(ss) | $(Mn_{0.22}Ti_{0.78})_3O_5$ |
| | + Reduced rutile | $(Mn_{0.02}Ti_{0.98})O_{1.95}$ |
| $10^{-14.91}$ | $M_3O_5$(ss) | $(Mn_{0.16}Ti_{0.84})_3O_5$ |
| | + Magneli phase | $(Mn_{0.011}Ti_{0.989})_8O_{15}$ |
| | + Magneli phase | $(Mn_{0.019}Ti_{0.981})_7O_{13}$ |
| $10^{-14.98}$ | $M_3O_5$(ss) | $(Mn_{0.15}Ti_{0.95})_3O_5$ |
| | + Magneli phase | $(Mn_{0.013}Ti_{0.987})_7O_{13}$ |
| | + Magneli phase | $(Mn_{0.025}Ti_{0.975})_6O_{11}$ |
| $10^{-15.48}$ | $M_3O_5$(ss) | $(Mn_{0.12}Ti_{0.88})_3O_5$ |
| | + Magneli phase | $(Mn_{0.006}Ti_{0.994})_6O_{11}$ |
| | + Magneli phase | $(Mn_{0.019}Ti_{0.981})_5O_9$ |
| $10^{-15.55}$ | $M_3O_5$(ss) | $(Mn_{0.115}Ti_{0.885})_3O_5$ |
| | + Magneli phase | $(Mn_{0.017}Ti_{0.983})_5O_9$ |
| | + Magneli phase | $(Mn_{0.030}Ti_{0.970})_4O_7$ |
| $10^{-17.2}$ | $M_3O_5$ | $(Mn_{0.11}Ti_{0.89})_3O_5$ |
| | + Tagirovite(ss) | $(Mn_{0.12}Ti_{0.88})_2O_{3.02}$ |
| | + Pyrophanite(ss) | $(Mn_{0.44}Ti_{0.56})_2O_{3.02}$ |
| $10^{-18.2}$ | Spinel(ss) | $(Mn_{0.43}Ti_{0.57})_3O_4$ |
| | + Tagirovite(ss) | $(Mn_{0.12}Ti_{0.88})_2O_3$ |
| | + Pyrophanite(ss) | $(Mn_{0.44}Ti_{0.56})_2O_3$ |

different phases. Oxygen contents were calculated from chemical analyses for $Mn^{2+}$, $Ti^{3+}$, and $Ti^{4+}$ in the quenched products, and any significant deviations from stoichiometry of the phases shown in Fig. 2 are discussed below. The data for the invariant points are listed in Table I.

Figure 2 shows a negligible solubility of titanium in $MnO_{1+x}$, an $\alpha$-oxide solid solution with a large miscibility gap, and extensions of the titanium oxides $Ti_nO_{2n-1}$, $n = 3$–8, by incorporation of manganese. The various solid-solution series are discussed in detail below.

### *5.1. Reduced Rutile Magneli Phases*

The Magneli Phase region (cf. Fig. 2) is reproduced on a larger scale in Fig. 3, where the data are for samples equilibrated by reduction of $Mn_2O_3 + TiO_2$ mixtures. In some runs we equilibrated different samples by oxidation and reduction paths and observed a hysteresis effect similar to that previously

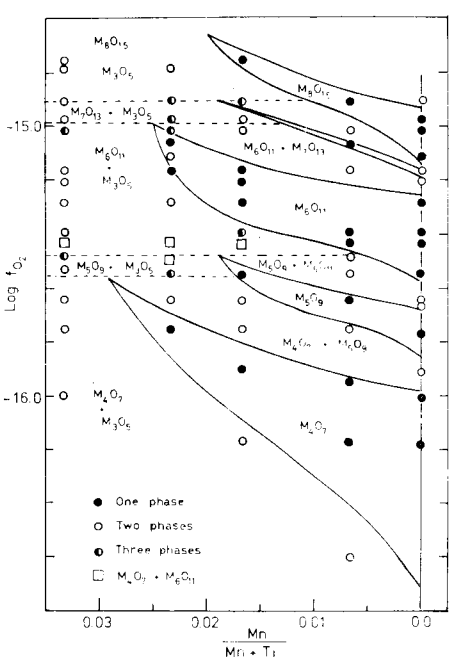


FIG. 3. Oxygen fugacity vs composition for the Magneli phase region of the Mn–Ti–O system at 1473°K. Samples were equilibrated by reduction of $Mn_2O_3$ plus $TiO_2$ mixtures. Bivariant behavior in the binary Ti–O system is shown at Mn/(Mn + Ti) = 0.0.

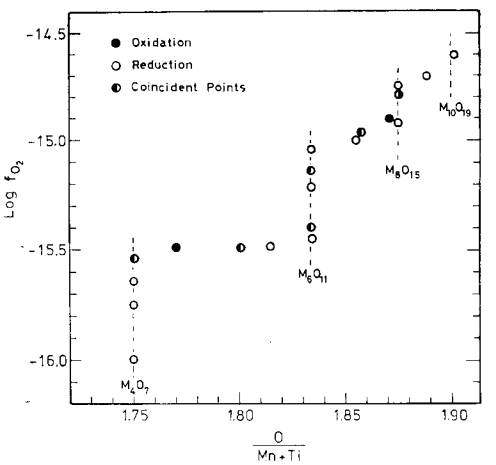


FIG. 4. Oxygen fugacity vs oxygen-to-metal ratio, O/(Mn + Ti), for Mn–Ti–O at 1473°K: equilibrium of Magneli phases with $M_3O_5$(ss) at a fixed Mn/(Mn + Ti) ratio of 0.067.

reported in the Ti–O and Fe–Ti–O systems (*6*); i.e., the samples equilibrated by oxidation had a lower O/(Mn + Ti) ratio than those equilibrated by reduction at the same oxygen fugacity. Bivariant behavior was also observed. The magnitude of both the hysteresis and the bivariant behavior decreased with increasing manganese content of the Magneli phases. This is illustrated in Fig. 4, where $\log f_{O_2}$ vs O/(Mn + Ti) is plotted for a Mn/(Mn + Ti) ratio of 0.06. At this value of the metal ratio, the Magneli phases are all in equilibrium with $M_3O_5$(ss) (see Fig. 2), and the reduction and oxidation paths coincide.

The solubility of manganese in the Magneli phases, $M_nO_{2n-1}$, increases with decreasing $n$ from 1.4 wt% in $M_8O_{15}$ to 1.8% in $Ti_6O_{11}$ and to 2.2% in $M_4O_7$. For the odd numbered homologues, $M_5O_9$ and $M_7O_{13}$, the maximum solubilities for manganese are about 1.4 and 1.3 wt% respectively, i.e. lower than for their adjacent $n$-even homologs. Also, as shown in Figs. 3 and 4, the oxygen fugacity ranges are much narrower for single phase (Ti, Mn)$_5O_9$ and (Ti, Mn)$_7O_{13}$ than for (Ti, Mn)$_4O_7$, (Ti, Mn)$_6O_{11}$, and (Ti, Mn)$_8O_{15}$. A similar greater stability of $n$-even homologs relative to $n$-odd members has previously been reported for Magneli phases in the Fe–Ti–O system (*6*).

TABLE II

LATTICE PARAMETERS FOR MAGNELI PHASES, $(Mn_xTi_{1-x})_nO_{2n-1}$

| Compositions | $\log f_{O_2}$ (atm) | Lattice parameters | | | | | |
|---|---|---|---|---|---|---|---|
| | | $a$ (Å) | $b$ (Å) | $c$ (Å) | $\alpha$ (°) | $\beta$ (°) | $\gamma$ (°) |
| $Ti_4O_7$ | −16.17 | 5.593(1) | 7.119(1) | 12.452(3) | 95.06(1) | 95.12(1) | 108.75(1) |
| $Ti_4O_7$ (*25*) | | 5.593(1) | 7.125(1) | 12.456(3) | 95.02(1) | 95.21(1) | 108.73(1) |
| $(Mn_{0.017}Ti_{0.983})_4O_7$ | −15.90 | 5.597(4) | 7.118(5) | 12.424(9) | 95.06(3) | 95.02(3) | 108.79(3) |
| $(Mn_{0.023}Ti_{0.977})_4O_7$ | −15.75 | 5.610(2) | 7.123(2) | 12.466(3) | 95.04(1) | 95.22(1) | 108.74(1) |
| $Ti_5O_9$ | −15.76 | 5.563(2) | 7.110(3) | 8.853(3) | 97.48(1) | 112.36(2) | 108.52(1) |
| | −15.80 | 5.568(1) | 7.117(1) | 8.861(2) | 97.54(1) | 112.35(1) | 108.54(1) |
| | −15.95 | 5.566(2) | 7.119(2) | 8.863(3) | 97.49(1) | 112.35(1) | 108.52(1) |
| $Ti_5O_9$ (*3*) | | 5.569 | 7.120 | 8.865 | 97.55 | 112.34 | 108.50 |
| $(Mn_{0.017}Ti_{0.983})_5O_9$ | −15.50 | 5.574(3) | 7.112(3) | 8.872(4) | 97.52(2) | 112.43(2) | 108.48(2) |
| $Ti_6O_{11}$ (*22*) | | 5.56 | 7.14 | 24.04 | 98.5 | 120.8 | 108.5 |
| $(Mn_{0.023}Ti_{0.977})_6O_{11}$ | −15.16 | 5.561(2) | 7.130(3) | 24.055(9) | 98.46(1) | 120.84(1) | 108.49(1) |
| $Ti_7O_{13}$ (*22*) | | 5.54 | 7.13 | 15.36 | 98.9 | 125.5 | 108.5 |
| $(Mn_{0.017}Ti_{0.983})_7O_{13}$ | −14.95 | 5.545(4) | 7.130(5) | 15.365(10) | 98.96(1) | 125.48(2) | 108.43(1) |
| $Ti_8O_{15}$ (*22*) | | 5.57 | 7.10 | 37.46 | 97.2 | 128.8 | 109.6 |
| $Ti_8O_{15}$ | | 5.530(2) | 7.134(3) | 37.59(1) | 99.13(1) | 128.34(1) | 108.51(1) |

Chemical analyses carried out on a number of samples shown by X-ray diffraction to be single phase were consistent with a formulation as solid solutions of the type $Ti_nO_{2n-1}$–$MnTi_{n-1}O_{2n-1}$, i.e., Magneli-phase solid solutions formed by the partial substitution of $Ti_2O_3$ by $MnTiO_3$ in $(Ti_2O_3)(TiO_2)_{n-2}$. All lines of the powder patterns of the manganese containing phases could be indexed using the unit cells given by Andersson and Jahnberg (*22*) for $Ti_nO_{2n-1}$. Some examples of calculated cell parameters are given in Table II. Incorporation of manganese leads to a slight expansion of the unit cells. From chemical analyses, the O/(Mn + Ti) ratios were calculated for a number of single phase samples, and were found to agree within ±0.005 with those expected for stoichiometric $(Mn, Ti)_nO_{2n-1}$.

In the reduced rutile region, alternate one- and two-phase reduced rutile regions were not resolved for O/(Mn + Ti) ratios above 1.888, i.e., $(Mn, Ti)_9O_{17}$. For reduced rutiles with higher O/(Mn + Ti) ratios the X-ray powder diffraction line positions changed continuously as the oxygen fugacity was varied. The solubility of manganese in these phases was almost independent of the oxygen fugacity at about 1.5 wt%. At an oxygen fugacity of $10^{-13.95}$ atm a reduced rutile of composition $(Mn_{0.02}Ti_{0.98})O_{1.95}$ is in equilibrium both with $M_3O_5$(ss) of composition $(MnTi_2O_5)_{0.65}(Ti_3O_5)_{0.35}$ and with α-oxide with composition close to $MnTiO_3$.

### 5.2. $M_3O_5$ Solid Solution

An $M_3O_5$(ss) solid solution is shown in Fig. 2 to extend from the titanium end-member, $Ti_3O_5$, to $Mn_{0.65}Ti_{2.35}O_5$, which, as stated above, is in equilibrium with reduced rutile and α-oxide at the invariant oxygen fugacity of $10^{-13.95}$ atm. At oxygen fugacities above $10^{-13.95}$ atm the $M_3O_5$(ss) is *unstable* relative to a phase assemblage containing α-oxide plus reduced rutile.

The range of oxygen nonstoichiometry of the $M_3O_5$(ss) was studied using the sealed tube method. Solid solution compositions with variable oxygen content, $Mn_xTi_{3-x}O_{5\pm\delta}$, $x = 0$–$0.65$ and $\delta = 0$–$0.05$, were prepared and equilibrated in sealed silica tubes. For compositions with $\delta$ greater than about 0.02 the X-ray diffractograms always showed a second phase present: reduced rutile for $\delta$

TABLE III

LATTICE PARAMETERS FOR MEMBERS OF THE $Mn_xTi_{3-x}O_5$ SOLID SOLUTION

| Compositions | $\log f_{O_2}$ (atm) | Lattice parameters | | | |
|---|---|---|---|---|---|
| | | $a$ (Å) | $b$ (Å) | $c$(Å) | $\beta$(°) |
| $Mn_{0.65}Ti_{2.35}O_5$ | −14.15 | 9.875(2) | 3.770(1) | 10.130(2) | |
| | Sealed tube | 9.873(2) | 3.772(1) | 10.131(2) | |
| $Mn_{0.60}Ti_{2.40}O_5$ | −15.04 | 9.868(3) | 3.776(1) | 10.104(3) | |
| | Sealed tube | 9.867(3) | 3.773(1) | 10.112(3) | |
| $Mn_{0.55}Ti_{2.45}O_5$ | −14.78 | 9.877(3) | 3.782(1) | 10.100(3) | |
| $Mn_{0.50}Ti_{2.50}O_5$ | −15.04 | 9.868(3) | 3.778(1) | 10.091(3) | |
| | −15.45 | 9.869(3) | 3.782(1) | 10.088(3) | |
| $Mn_{0.40}Ti_{2.60}O_5$ | −15.45 | 9.863(2) | 3.785(1) | 10.067(2) | |
| | −15.88 | 9.854(3) | 3.781(1) | 10.058(2) | |
| | −16.70 | 9.860(2) | 3.777(1) | 10.057(2) | |
| $Mn_{0.34}Ti_{2.66}O_5$ | −16.80 | 9.860(2) | 3.783(1) | 10.030(2) | |
| | −17.5 | 9.860(2) | 3.782(1) | 10.030(2) | |
| | −17.3 | 9.872(3) | 3.784(1) | 10.044(3) | |
| $Mn_{0.30}Ti_{2.70}O_5$ | −15.88 | 9.851(2) | 3.783(1) | 10.034(2) | |
| $Mn_{0.30}Ti_{2.70}O_{4.97}$[a] | Sealed tube | 9.857(2) | 3.783(1) | 10.023(2) | |
| $Mn_{0.30}Ti_{2.70}O_{5.02}$[a] | Sealed tube | 9.855(2) | 3.784(1) | 10.043(2) | |
| $Mn_{0.20}Ti_{2.80}O_5$ | −16.80 | 9.848(3) | 3.783(1) | 10.013(3) | 90.54(1) |
| $Mn_{0.14}Ti_{2.86}O_5$ | −16.80 | 9.831(3) | 3.782(1) | 9.989(3) | 90.68(1) |
| $Mn_{0.05}Ti_{2.95}O_5$ | −16.80 | 9.827(3) | 3.785(1) | 9.970(3) | 91.02(1) |
| $Ti_3O_5$[b] | | 9.82 | 3.78 | 9.97 | 91.0 |

[a] Second phase observed in X-ray patterns.
[b] From Ref. (*26*).

positive or α-oxide for $\delta$ negative. It is concluded that $M_3O_5$(ss) has a very narrow range of homogeneity at 1473°K, $MO_{1.667\pm0.005}$. Refined values of lattice parameters for a number of well-characterized members of the solid solution series are given in Table III. For samples prepared at low oxygen fugacities, the variation in the refined parameters for different preparations were sometimes an order of magnitude larger than the standard deviations estimated for the known phases. This is attributed to a nonequilibrium situation applying at low oxygen fugacities, when there is relatively rapid vaporization of metallic manganese from the sample. In Fig. 5 the lattice parameters for characterized members of the $M_3O_5$(ss) series are plotted as a function of composition. It is seen that replacement of $2Ti^{3+}$ by $Mn^{2+} + Ti^{4+}$ leads to an expansion of the unit cell due both to the large size of the divalent manganese ion and also to the breakdown of metal–metal bonding between pairs of trivalent titaniums, cf. (*23*). Also apparent from Table III is a change from orthorhombic to monoclinic symmetry as the manganese content decreases. The monoclinic distortion was first discernible in the X-ray patterns at the composition $Mn_{0.20}Ti_{2.80}O_5$.

### *5.3. α-Oxide Solid Solution*

Figure 2 shows a large miscibility gap in the α-oxide solid solution for the Mn/(Mn + Ti) range 0.44–0.12. To avoid confusion, the manganese-rich series is called pyrophanite(ss) while the titanium-rich series, close to $Ti_2O_3$, is called tagirovite(ss) (*24*). The pyrophanite(ss) is unstable relative to mixtures of spinel and tagirovite(ss) at oxygen fugacities below about $10^{-18}$ atm. Because of the difficulties discussed in Section 4 there is

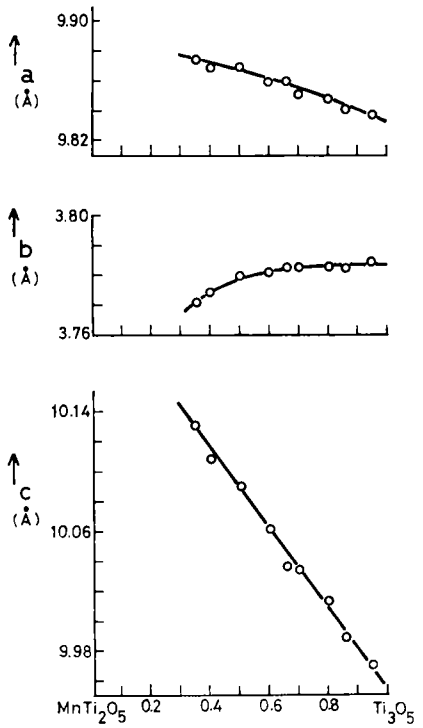


FIG. 5. Variation of lattice parameters with composition in the series $Mn_xTi_{3-x}O_5$.

considerable uncertainty associated with the region. This is indicated by the dotted phase boundaries in Fig. 2. The tagirovite(ss) is unstable relative to pyrophanite(ss) plus $M_3O_5$(ss) at oxygen fugacities *above* $10^{-17.2}$ atm. For fugacities between $10^{-17.2}$ and $10^{-18.2}$ atm, the pyrophanite(ss) and tagirovite(ss) coexist as an equilibrium phase assemblage for Mn/(Mn + Ti) ratios between 0.12 and 0.44.

### *5.4. Spinel Solid Solution*

The lower boundary of the spinel(ss) in equilibrium with $MnO_{1+x}$ remained almost unchanged over the oxygen fugacity range, at a composition close to $Mn_2TiO_4$. The upper boundary, of spinel(ss) in equilibrium with α-oxide(ss), moved to lower Mn/(Mn + Ti) ratios as the oxygen fugacity decreased. For a sample equilibrated in flowing hydrogen with an oxygen fugacity less than $10^{-18}$ atm the boundary of the spinel(ss) was $(MnTi_2O_4)_{0.80}(Mn_2TiO_4)_{0.20}$. Lecerf et al. (*14*) have shown, from sealed tube studies, that the solid solution between $MnTi_2O_4$ and $Mn_2TiO_4$ is complete at 1473°K. The $MnO_{1+x}$ phase showed negligible solubility for titanium oxide over the oxygen fugacity range $10^{-13.5}$–$10^{-18}$ atm. Mixtures with Mn/(Mn + Ti) ratios of 0.975 always contained spinel(ss) as a second phase.

## 6. Comparison of Phase Equilibria in the $FeO$–$TiO_2$–$Ti_2O_3$ and $MnO$–$TiO_2$–$Ti_2O_3$ Systems

The results of the controlled oxygen fugacity studies on the reduced rutile and $M_3O_5$(ss) compounds have been used, together with the results of chemical analyses on the quenched products, to derive an isothermal composition diagram for the section of the Mn–Ti–O system bounded by $TiO_2$, $Ti_3O_5$, and "$MnTi_2O_5$". This is shown in Fig. 6. The data obtained for samples equilibrated by reduction of $TiO_2 + Mn_2O_3$ mixtures are shown in this figure.

It is instructive to compare the phase equilibria in Fig. 6 with the corresponding equilibria in the $FeO$–$Ti_2O_3$–$TiO_2$ system as shown in Fig. 7. It is apparent that in the oxide structures studied, the thermodynamic stabilities of the two ions $Fe^{2+}$ and $Mn^{2+}$ are considerably different. While this may be partly due to differences in their ionic radii, $r_{Fe^{2+}} = 0.78$ Å and $r_{Mn^{2+}} = 0.83$ Å (*27*), it appears to be primarily a reflection of the much lower free energy of formation of $Fe_{0.95}O$ as compared with MnO and the consequent ease of reduction of oxide compounds of $Fe^{2+}$ in general as compared with those of manganese. Thus, in phase assemblages containing trivalent titanium, ferrous iron is unstable and is easily reduced to the metal. The equilibrium $2Ti^{3+} + Fe^{2+} \rightarrow 2Ti^{4+} + Fe^{\circ}$ lies very much to the right, and lattice stabilization energies allow only a fraction of 1% of ferrous iron in most of the trivalent titanium-containing oxides. The effect is most apparent in a comparison of $M_3O_5$ compositions. $Ti_3O_5$ will incorporate 15.6 wt% manganese in a solid solution of the type $(Ti_3O_5)_x(MnTi_2O_5)_{1-x}$, whereas only 0.6 wt% of ferrous iron is soluble in $Ti_3O_5$. Beyond this the solid

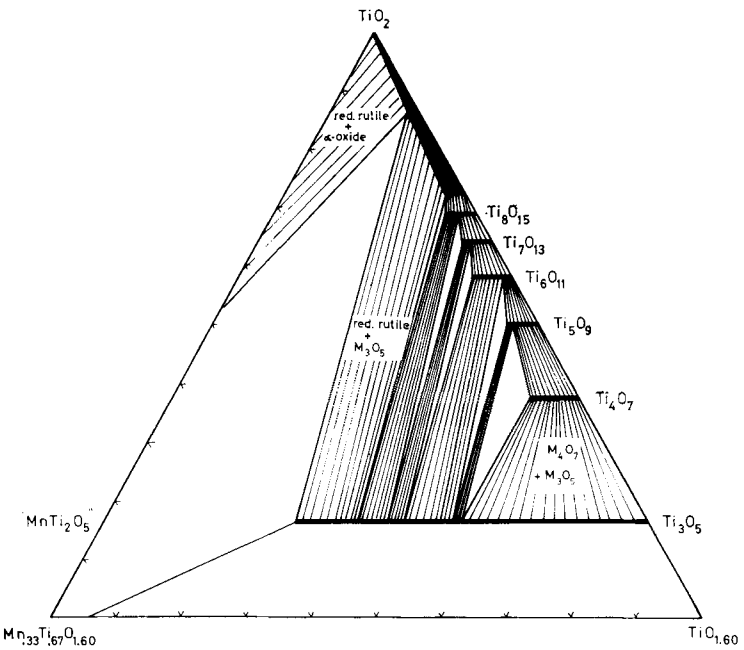


FIG. 6. Isothermal section of the Mn–Ti–O phase diagram at 1473°K, showing the composition region bounded by $TiO_2$, $Ti_3O_5$, and "$MnTi_2O_5$." Compositions are given in mole percent. Details of compositions and oxygen fugacities are given in Table I.

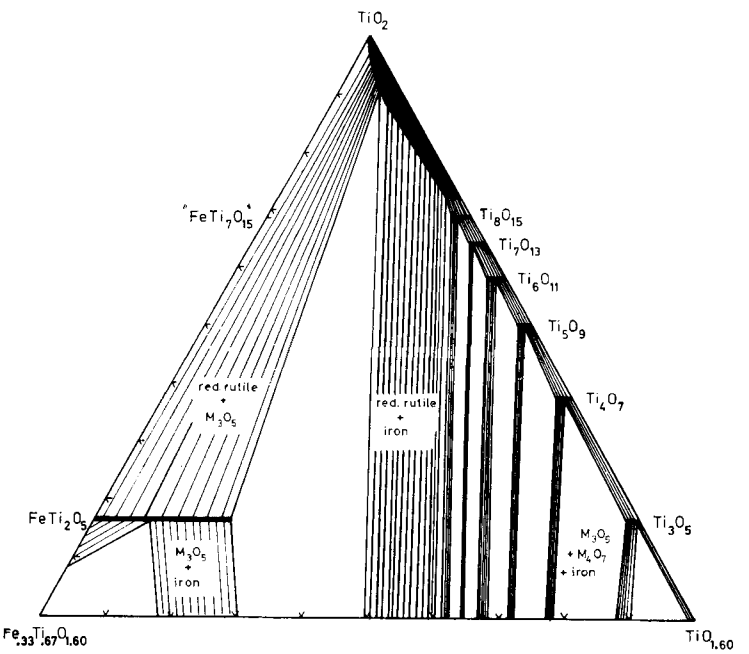


FIG. 7. Isothermal section of part of the Fe–Ti–O phase diagram at 1473°K, showing details of the composition region bounded by $TiO_2$, $Ti_3O_5$, and $FeTi_2O_5$. Compositions are given in mole percent. Data used in Fig. 7 are taken from (*1*) and (*6*).

solution is unstable relative to a mixture of metallic iron and an oxide with a lower $Ti^{3+}$ content, $M_4O_7$. It is interesting that the thermodynamic behaviour of the $FeTi_2O_5$–$Ti_3O_5$(ss) almost exactly complements that of the $MnTi_2O_5$–$Ti_3O_5$ series. Thus, whereas the former solid solution is stable only *above* an oxygen fugacity of $10^{-13.95}$ atm, the latter solid solution is stable only *below* the same value of the oxygen fugacity.

The different thermodynamic stabilities of $Mn^{2+}$ and $Fe^{2+}$ in reduced oxide assemblages are also seen by a comparison of the Magneli phase regions. Thus, while the solubility of manganese in the Magneli phases $M_nO_{2n-1}$ increases with decreasing $n$, the reverse is true for iron. We have previously reported the combining of the phase equilibria data for the Fe–Ti–O and the Mn–Ti–O systems to interpret the effect of manganese on ilmenite reduction (*1*).

## Acknowledgments

The authors are indebted to Consolidated Gold Fields Australia Ltd. for support of the work reported in this paper. Special thanks are due to Dr. A. G. Turnbull for help with thermodynamic computing and for making his programs for equilibria calculation available.

## References

1. I. E. Grey, A. F. Reid, and D. G. Jones, *Inst. Mining Met. Trans., Sect. C* **83**, C105 (1974).
2. I. E. Grey and A. F. Reid, *Inst. Mining Met. Trans., Sect. C* **83**, C39 (1974).
3. S. Andersson, B. Collen, V. Kuylenstierna, and A. Magneli, *Acta Chem. Scand.* **11**, 1641 (1957).
4. P. G. Wahlbeck and P. W. Gilles, *J. Amer. Ceram. Soc.* **49**, 180 (1966).
5. V. R. Porter, Ph.D. Thesis, Pennsylvania State University, 1965.
6. I. E. Grey, C. Li, and A. F. Reid, *J. Solid State Chem.* **11**, 120 (1974).
7. J. S. Anderson and A. S. Khan, *J. Less-Common Metals* **22**, 219 (1970).
8. R. R. Merritt and B. G. Hyde, *Philos. Trans Roy. Soc. London, Ser. A* **274**, 627 (1973).
9. N. J. Bogdanova, G. P. Pirogovskaya, and S. M. Ariya, *Russ. J. Inorg. Chem.* **8**, 401 (1963).
10. K. Suzuki and K. Sambongi, *Tetsu To Hagane* **58**, 1579 (1972).
11. L. A. Bursill and B. G. Hyde, *Progr. Solid State Chem.* **7**, 177 (1972).
12. B. E. F. Fender and F. D. Riley, "The Chemistry of Extended Defects in Non-Metallic Solids," pp. 54–61, North-Holland, Amsterdam (1970).
13. J. Grieve and J. White, *J. Roy. Tech. Coll. Glasgow* **4**, 661 (1940).
14. A. Lecerf, M. Rault, and G. Villers, *C.R. Acad. Sci.* **261**, 749 (1965).
15. L. S. Darken and R. W. Gurry, *J. Amer. Chem. Soc.* **67**, 1398 (1945).
16. A. H. Webster and N. F. H. Bright, *J. Amer. Ceram. Soc.* **44**, 110 (1961).
17. H. H. Kellog, *Trans. Met. Soc. A.I.M.E.* **236**, 602 (1966).
18. S. A. Jansson and E. A. Gulbransen. "Evaluation of Gas–Metal Reactions by Means of Thermochemical Diagrams," paper presented at the International Congress on Corrosion, Amsterdam, September 1969.
19. "Selected Values of Chemical Thermodynamic Properties," *Nat. Bur. Stand. (U.S.) Tech. Note* 270 (1969).
20. K. K. Kelley, *U.S. Bur. Mines Bull.* 584 (1960).
21. R. Hultgren, R. C. Orr, P. D. Anderson, and K. K. Kelley. "Selected Values of Thermodynamic Properties of Metals and Alloys," Wiley, New York (1963).
22. S. Andersson and L. Jahnberg, *Ark. Kemi* **21**, 413 (1963).
23. I. E. Grey and J. Ward, *J. Solid State Chem.* **7**, 300 (1973).
24. V. A. Reznichenko and T. P. Ukolva, *Titan Ego Splavy* 80 (1961).
25. M. Marezio, D. B. McWhan, P. D. Dernier, and J. P. Remeika, *J. Solid State Chem.* **6**, 213 (1973).
26. S. Asbrink and A. Magneli, *Acta Crystallogr.* **12**, 575 (1959).
27. R. D. Shannon and C. T. Prewitt, *Acta Crystallogr., Sect. B* **25**, 925 (1969).